# Rapid thermal treatment of oriented microstructures to generate fine globular grains

Sathyanarayan Sairam Jaishankar<sup>1</sup>, Donggang Yao<sup>1,3</sup>, Jack G. Zhou<sup>2</sup>

- 1. School of Materials Science and Engineering, Georgia Institute of Technology, Atlanta, GA 30332, USA.
- 2. Department of Mechanical Engineering and Mechanics, Drexel University, Philadelphia, PA 19104, USA.
  - 3. e-mail: yao@gatech.edu

#### **Abstract**

Metal additive manufacturing through fused filament fabrication (FFF) is recently gaining traction owing to its simplicity, cost benefit, and suitability to a wide range of starting materials, as compared to alternative technologies. The generation of a thixotropic (globular) microstructure is fundamental to obtaining the desired flow behavior in the semi-solid material. Although numerous studies have explored the possibility to print extruded filaments, a scalable process for manufacturing 3D-printable filaments is yet to be established. Drawn filaments possess similar microstructures to extruded filaments and are commercially produced. In this study, we demonstrate that small globular grains (~10µm) can be generated in a cold-drawn filament of a Zn-Al alloy using rapid thermal treatment. The filaments were heated to different temperatures (375, 385, 400, 420, and 450°C) using a molten salt bath. The larger heat transfer coefficient of the molten salt bath, compared to convective heating, drastically reduced the time required to achieve the target temperature to a few seconds. Higher set temperatures led to quicker transformation into globular microstructure due to Rayleigh instability and resulted in smaller initial grain sizes. Longer treatment times promoted grain coarsening due to Ostwald ripening. Such a pretreatment may enable fine resolution printing using thixotropic filaments.

# **Keywords**

Drawn wire, semi-solid metal processing, additive manufacturing, thixotropic microstructure, globular grains, rapid thermal treatment

## Introduction

Semi-solid metal processing (SSMP) refers to a variety of processing techniques that enable near-net-shape manufacturing of metal parts. They differ from conventional metal processing techniques in that they produce complex geometries from semi-solid materials [1,2]. Metal alloys containing a two-phase semi-solid region can be processed into a viscous slurry that exhibits flow behavior similar to thermoplastic materials. These two-phase slurries undergo a time-dependent shear-thinning behavior when subjected to shear forces [3]. This phenomenon is termed thixotropy and processes that employ such rheological behavior for producing metal parts are termed as thixotropic processes. The microstructure that is essential to impart thixotropic properties to the semi-solid slurry is referred to as a thixotropic microstructure. It consists of globular grains of solid phase uniformly distributed in the liquid phase matrix. Unlike dendritic grains, the globular grains can slide past each other when a shear force is applied, thereby offering reduced resistance to flow [4]. Upon removal of the applied shear, the viscosity rapidly builds to its initial value, which is essential to maintain the shape of the formed product.

The advantages of SSMP techniques include minimal part shrinkage upon solidification, lower operating temperatures compared to conventional casting, and reduced tool and die wear [2]. SSMP techniques can be classified as rheoforming or thixoforming techniques. Rheoforming techniques such as rheocasting and rheomolding generate thixotropic (globular) microstructure by applying a shear force through mechanical stirring or rotating screws to a liquid alloy under cooling [5]. This ensures that the grains formed in the semi-solid region are equiaxed. Rice et al. [6] successfully demonstrated the freeform fabrication of parts from a low melting Sn-Pb alloy using a continuous rheocasting process. Commercially, parts made

from Mg alloys are manufactured using rheomolding or high pressure die casting. In either process, a thixotropic slurry is usually generated in a twin-screw slurry maker and is injected into the mold cavity under pressure in a controlled manner [7]. The major limitations of rheoforming techniques pertain to bulky equipment, accurate temperature control, cleanness of processing equipment, and the need for high shear rates to generate fine globular microstructure.

On the other hand, thixoforming techniques such as thixocasting, thixoforging, and thixomolding generate globular microstructure by heating billets/chips to the semi-solid temperature range of the alloy. The billets may already contain the globular microstructure prior to partial melting if they are rheocast [4]. Alternately, the cast billets containing dendritic grains may be subjected to severe plastic deformation to prepare them for thixotropic processing. To create a thixotropic material from solid feedstock, a multi-step process is usually employed. In the first step, the coarse, dendritic cast microstructure is converted into a fine equiaxed microstructure. It is commonly achieved by hot and cold working under the Strain-Induced Melt Activation (SIMA) protocol or warm working (below the recrystallization temperature) under the Recrystallization and Partial Melting (RAP) method. Compression [8,9], extrusion [10,11,12,13], swaging [14], and equal channel angular pressing [15], among other processes may be used to refine the grains and store sufficient strain energy in the material prior to the reheating step. In the second step, the strained material is heated to a temperature in the semi-solid range to produce globular grains surrounded by a liquid matrix.

Globular microstructures generated from thixoforming or rheoforming techniques demonstrate remarkable improvement in mechanical properties such as hardness, strength, and ductility, as compared to cast microstructures [16,17]. Thixotropic microstructures are also key to achieving desirable rheological behavior for FFF of metallic materials. The small nozzle geometry of the printheads necessitates fine globular grains to be developed during the reheating step. The filament used in the FFF process is typically produced by extrusion. Alharbi et al. [18] investigated a heat treatment processing window for producing globular microstructure in extruded wires of a Pb-40%Sn alloy. Jabbari et al. [19,20] introduced a pretreatment step to generate globular microstructure in extruded filaments of different Pb-Sn alloys prior to the printing step. The pretreatment was conducted by heating the filaments supported inside a PTFE tube in an oven for the desired time at a specific temperature. It enabled controlled and precise deposition of layers from the thixoextruder, with an average grain size larger than 50µm. Lima et al. [21] successfully 3D-printed various shapes from an extruded filament of a Mg-Zn alloy using a novel printhead that could operate at 420°C. Globular grains generated in-situ during the printing step had small grain size (~5µm) and high mean circularity. Despite the successful results from these studies, an industrially scalable process to produce printable filaments was not demonstrated.

Literature survey revealed that filaments produced by commercial wire drawing processes have not been adequately studied for the production of thixotropic microstructures. One study by Nezic et al. [22] showed that welding wires of Al alloys could generate globular grains when subjected to heat treatment. The authors used a convection oven to heat the samples to the target temperature which resulted in a long treatment time ( $\sim$ 15 minutes) and large grain size ( $\sim$ 70 $\mu$ m). We also found no studies on rapid thermal treatments, either as a precursor to the printing step or during printing from literature analysis. Smaller grain sizes can enable fine resolution printing which would be essential for tiny geometries, intricate designs, and better surface finish. For this study, we selected a zinc-aluminum alloy (nominal composition Zn - 85%, Al - 15% by weight, hereafter referred to as Zn85Al15) drawn into a wire. These

wires are primarily used for thermal spray coating applications for galvanic protection of steel structures. Similar zinc alloy compositions are commonly used to make light-weight components through die-casting. Their balanced mechanical properties (high hardness, moderate strength, reasonable ductility) and excellent electrical and thermal properties promote their use in automotive and electrical components [23,24]. To the best of our knowledge, we found no literature on the use of Zn85Al15 wires for FFF or wire-arc additive manufacturing (WAAM). Therefore, a study to establish the suitability of zinc-aluminum alloys (particularly Zn85Al15) for the FFF process is desired. Through this study, we aim to demonstrate a rapid thermal treatment method for drawn filaments that can produce thixotropic microstructures with small grain size (~10μm).

## Materials and methods

Metallic wires of the Zn85Al15 alloy were obtained from The Platt Brothers and Company. The suitability of this alloy composition for thixotropic processing is explored in the following section. The wires had an average diameter of 0.091 inch (2.31 mm) and were prepared using a combination of drawing and rolling. Wires with an initial diameter of 0.3 inch were drawn to a diameter of approximately 0.165 inch through a series of lubricated dies and subsequently rolled in multiple passes to the final diameter. The wires are heated to nearly 180°F (~355K) due to friction during the drawing process, which is below the recrystallization temperature for this alloy composition (0.5T<sub>liquidus</sub> ~ 366K). Therefore, the wires are cold worked with sufficient degree of strain necessary for globular transformation.

Thermodynamic simulations to predict the liquid fraction profile in the semi-solid temperature range were performed using Thermocalc software (Thermo-Calc Software AB, Stockholm). Both equilibrium and non-equilibrium conditions were considered and correspondingly the phase diagram and Scheil solidification curve was generated for this alloy composition. Subsequently, multiple criteria were established to determine the temperature window for heat treatment of the alloy filaments. Three different temperatures satisfying these criteria (385, 400, and 420°C) were selected to study the evolution of globular microstructures within the alloy wires. Additionally, to understand the role of kinetic effects in the globularization behavior of the alloy, the heat treatments were also performed at 375 and 450°C. The heat treatments were conducted in a sodium nitrate salt bath contained in an alumina crucible and maintained at the target temperature in a furnace. Small pieces of the wire were immersed in the salt bath for a predetermined amount of time which was recorded using a stopwatch. Upon completion of the heating step, the wire fragments were quickly removed from the heating medium and immediately quenched in cold water. For each set temperature, the heat treatments were performed for different durations to identify the minimum time required for the start and completion of globular transformation at that temperature. These values were determined experimentally to be 2, 5s at 450°C, 5, 10s at 420°C, and 15, 20s at 400°C respectively. Separated globular grains were observed only after 90s of heating when the set temperature was 385°C. Longer heat treatments were also performed at 400 and 420°C to understand grain coarsening behavior in the semi-solid condition.

Salt bath heating is an industry standard technique for rapid and uniform heating of metal parts. Due to the large volume of the salt bath compared to the wire fragment and the high heat capacity of the salt bath and crucible, the change in temperature of the heating medium is assumed to be negligible. The heating of the wire in the salt bath can be analyzed using the lumped capacitance method. The principal assumption of this method is that the temperature

within a solid during transient heating/cooling is spatially uniform when the rate of heat conduction within the solid is much greater than the rate of heat flow into/out of it. In the absence of thermal gradients, the temperature of the entire solid is a function of time only. Thus, we can estimate the time required for the wire fragment to reach the target temperature using the following equation [25]—

$$\rho V c \frac{dT}{dt} = -hA(T - T_{\infty}) \tag{1}$$

where  $\rho$  is the density of the alloy, V is the volume of the wire fragment, c is the specific heat capacity of the alloy, h is the convective heat transfer coefficient of the salt bath, A is the total surface area of the wire fragment, and  $T_{\infty}$  is the set temperature of the heating bath.

Samples were prepared for microstructural analysis using standard metallographic techniques. The samples were set in epoxy and grinded using 120, 400, 800, and 1200 grit sandpapers. It was followed by polishing using oil-based diamond suspensions having particle sizes of 9, 3, and 1µm. A Phenom XL SEM with a four quadrant back-scattered detector was operated to observe the microstructure of the unetched samples. ImageJ software was used for quantitative analysis of the sample images. The grain areas and perimeters were obtained from the processed images and the average grain size and circularity were calculated for the different experimental parameters. The diameter of a grain was calculated according to the following formula [21]—

$$D = 2\sqrt{\frac{A}{\pi}} \tag{2}$$

Where A is the grain area. The circularity of a grain was calculated as [21]–

$$C = 4\pi \frac{A}{P^2} \tag{3}$$

where P is the grain perimeter.

## Results and discussions

# Thixotropic processing criteria

The general criteria for material selection for thixotropic processing involves achieving a desired liquid fraction interval during the partial remelting step, having low liquid fraction sensitivity to temperature changes at that liquid fraction, and having a small solidification interval to prevent hot tearing of the alloy during subsequent solidification. The desired liquid fraction interval depends on the processing and is usually between 0.3 to 0.5 for thixoforming techniques [26,27]. However, for FFF techniques, a low liquid fraction results in large extrusion forces while a high liquid fraction could promote droplet formation resulting in discontinuous printing. Therefore, for additive manufacturing, the desired liquid fraction range is between 0.5 - 0.8 [21]. The alloy composition is carefully selected to satisfy the above requirements. In this study, thermodynamic simulations were performed to guide temperature selection in the semi-solid range.

Fig. 1 presents the equilibrium phase diagram of a binary system of zinc and aluminum. The composition of the Zn85Al15 alloy is denoted by the vertical dashed line in the figure. The phase diagram indicates that the alloy is hypereutectoid but hypoeutectic. The eutectoid

transformation occurs at  $277^{\circ}\text{C}$  whereby the  $\beta$  phase decomposes into the Al-rich  $\alpha$  phase and the Zn-rich  $\eta$  phase during cooling. The eutectic reaction occurs at  $381^{\circ}\text{C}$  and results in the formation of the  $\beta$  and  $\eta$  phases from the solidifying liquid. The semi-solid range of the alloy under equilibrium conditions is obtained from the intersection of the dashed line with the solidus and liquidus curves. For the Zn85Al15 alloy, the solidus temperature is  $381^{\circ}\text{C}$  and the liquidus temperature is  $459^{\circ}\text{C}$ . The semi-solid temperature range is  $78^{\circ}\text{C}$ , which is below the threshold of  $150^{\circ}\text{C}$  to avoid hot tearing during cooling [28].

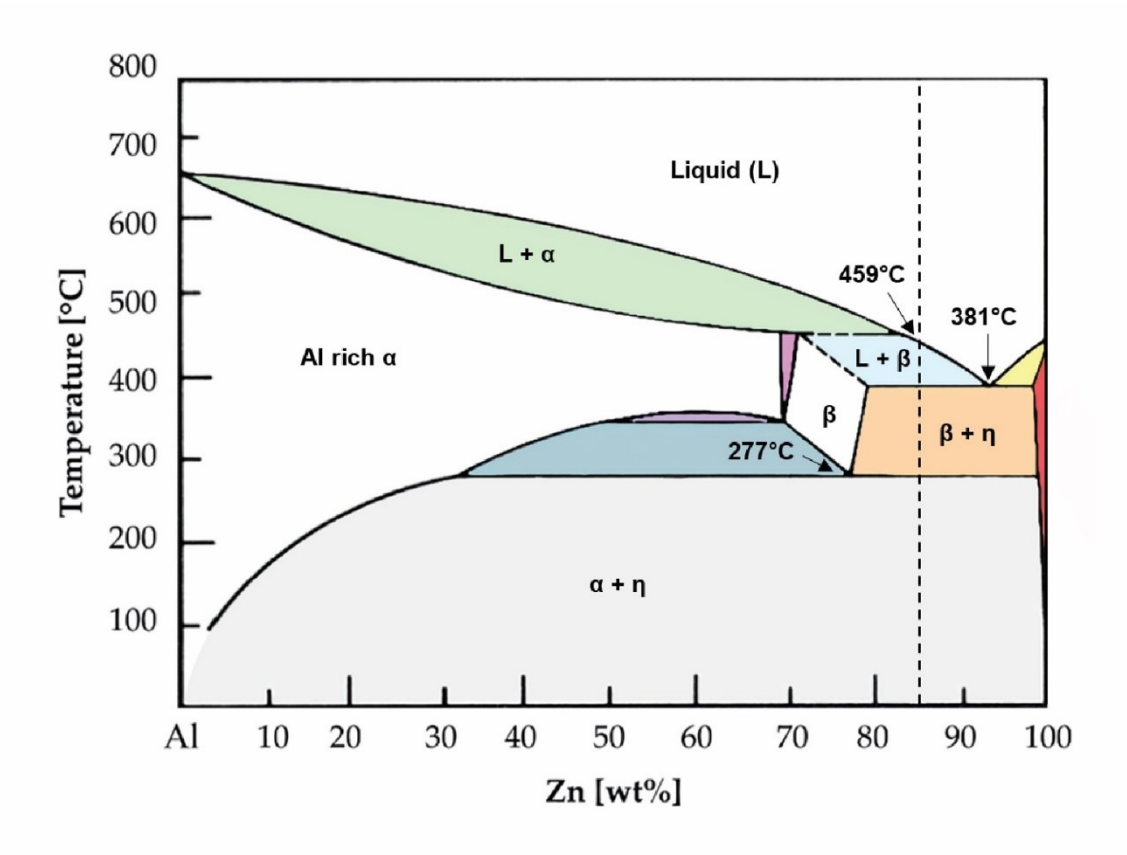


Fig. 1. Zinc – aluminum phase diagram as adapted from Pola et al. [24]. Vertical dashed line denotes the composition of the Zn85Al15 alloy.

The results from the Scheil simulation are presented in Fig. 2. Scheil solidification accounts for non-equilibrium conditions such as rapid cooling during the solidification process. It predicts the amount of solid and liquid phases in the system as a function of the temperature. For the Zn85Al15 alloy, the non-equilibrium simulation results are almost identical to the equilibrium results. The predicted solidus and liquidus temperatures are approximately 381°C and 459°C, with a semi-solid temperature range of 78°C. According to Liu et al. [26], the microstructure of materials prepared using the SIMA or RAP routes before partial remelting is expected to be quite uniform and devoid of cored structures. Therefore, they suggest that equilibrium predictions will most closely represent the phase composition at any temperature for such materials. Since the equilibrium and Scheil predictions for the semi-solid temperature range are similar for the Zn85Al15 alloy, we may infer that the alloy melting behavior is less susceptible to processing history. However, the liquid fraction evolution within the solidus-liquidus range may differ between the equilibrium and non-equilibrium predictions. Due to the transient temperatures within the sample during rapid thermal

treatment, we expect non-equilibrium conditions to prevail. Therefore, the liquid fraction profile predicted by the Scheil simulation will be considered for further analysis.

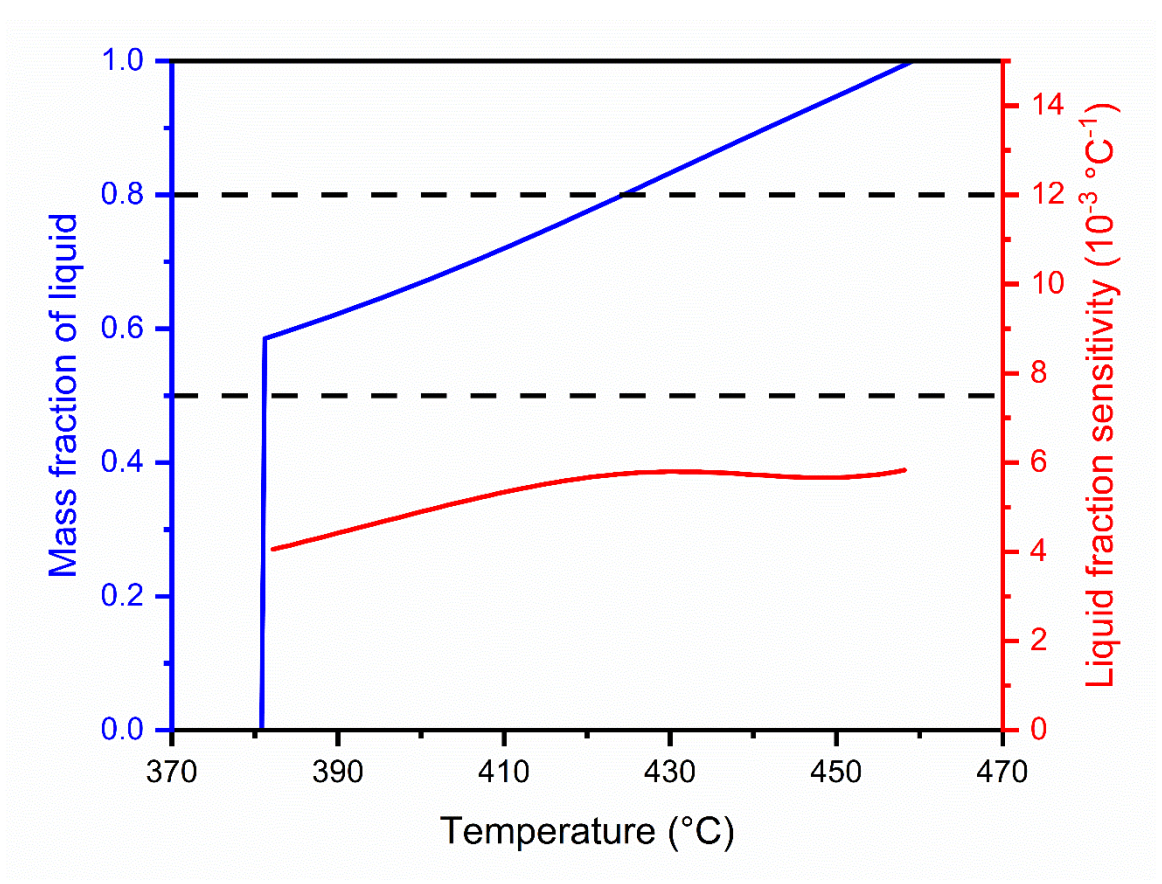


Fig. 2. Plot of mass fraction of liquid and liquid fraction sensitivity as a function of temperature under non-equilibrium (Scheil) conditions for the Zn85Al15 alloy. The horizontal dashed lines demarcate the ideal processing window for additive manufacturing corresponding to a liquid fraction range of 0.5 to 0.8.

Another important consideration is the liquid fraction sensitivity of the alloy in the desired processing temperature window. The liquid fraction sensitivity is defined as the change in liquid fraction per 1°C change in temperature. At temperatures above the knee (corresponding to eutectic meting), the change in liquid fraction occurs due to the gradual melting of the  $\beta$  phase grains. A low sensitivity (<  $0.015^{\circ}C^{-1}$ ) ensures that the liquid fraction does not change significantly with temperature fluctuations [21]. Since the viscosity of the semi-solid material is a function of the liquid fraction, it is crucial to ensure that the liquid fraction does not change appreciably during processing. For the Zn85Al15 alloy, the liquid fraction sensitivity varies between 0.004 to  $0.006^{\circ}C^{-1}$  throughout the semi-solid range, which is below the acceptable threshold of  $0.015^{\circ}C^{-1}$ . Therefore, this alloy satisfies the criteria to undergo thixotropic processing.

# Lumped capacitance analysis

Based on the thermodynamic simulations, five different temperatures were selected to study the globularization behavior – 375, 385, 400, 420, and 450°C. Among these, three temperatures (385, 400, and 420°C) fall within the ideal processing window for additive

manufacturing processes. The lowest and highest temperatures (375 and 450°C) help us better understand kinetic phenomenon during the transient heating. Since the wire fragments were heated to the target temperature in a salt bath, we can obtain a general analysis for the time required to reach the semi-solid range using the lumped capacitance method. Table I lists some properties of the Zn85Al15 alloy wire. It is essential that the Biot number be less than 0.1 for the material to be suitable for lumped capacitance analysis. It is calculated according to the equation [25]—

$$Bi = \frac{hL_c}{k} \tag{4}$$

where k is the thermal conductivity of the alloy, and  $L_c$  is the characteristic length of the wire fragment and is equal to r/2. We find that the Biot number is less than 0.1 for h up to 20000 J/(sm<sup>2</sup>K). The expected range of values of h for molten baths of sodium nitrate and its mixtures from literature analysis is 20 - 2000 J/(sm<sup>2</sup>K). Therefore, we may proceed with lumped capacitance analysis for our system.

Table I. Properties of the Zn85Al15 alloy wire. Magnitude of quantities denoted by \* are representative from a similar alloy composition, as adapted from [23].

| Quantity                | Symbol | Magnitude               | Units             |
|-------------------------|--------|-------------------------|-------------------|
| Diameter                | d      | 2.31*10 <sup>-3</sup>   | m                 |
| Radius                  | r      | 1.155*10 <sup>-3</sup>  | m                 |
| Length                  | l      | 2.54*10 <sup>-2</sup>   | m                 |
| Total surface area      | A      | 1.927*10 <sup>-4</sup>  | m <sup>2</sup>    |
| Volume                  | V      | 1.0645*10 <sup>-7</sup> | m <sup>3</sup>    |
| Density*                | ρ      | 6*10 <sup>3</sup>       | kg/m <sup>3</sup> |
| Specific heat capacity* | С      | 450                     | J/(kg*K)          |
| Thermal conductivity*   | k      | 120                     | J/(s*m*K)         |

Although the lumped capacitance technique does not account for the energy of phase transformations and latent heat for partial melting, it provides a fair estimate of the temperature of the wire at a given time. Fig. 3 illustrates the time required for the wire to reach the semi-solid temperature range for different values of h at a constant bath temperature of 450°C. The higher the value of h, shorter is the time required and vice versa. While we did not determine the heat transfer coefficient from our experiments, it would be essential in commercial setups to precisely control the heat treatment process. The set temperature also influences the time required to reach the semi-solid range. The lower the set temperature, higher is the time required since the temperature rises asymptotically from the initial temperature.

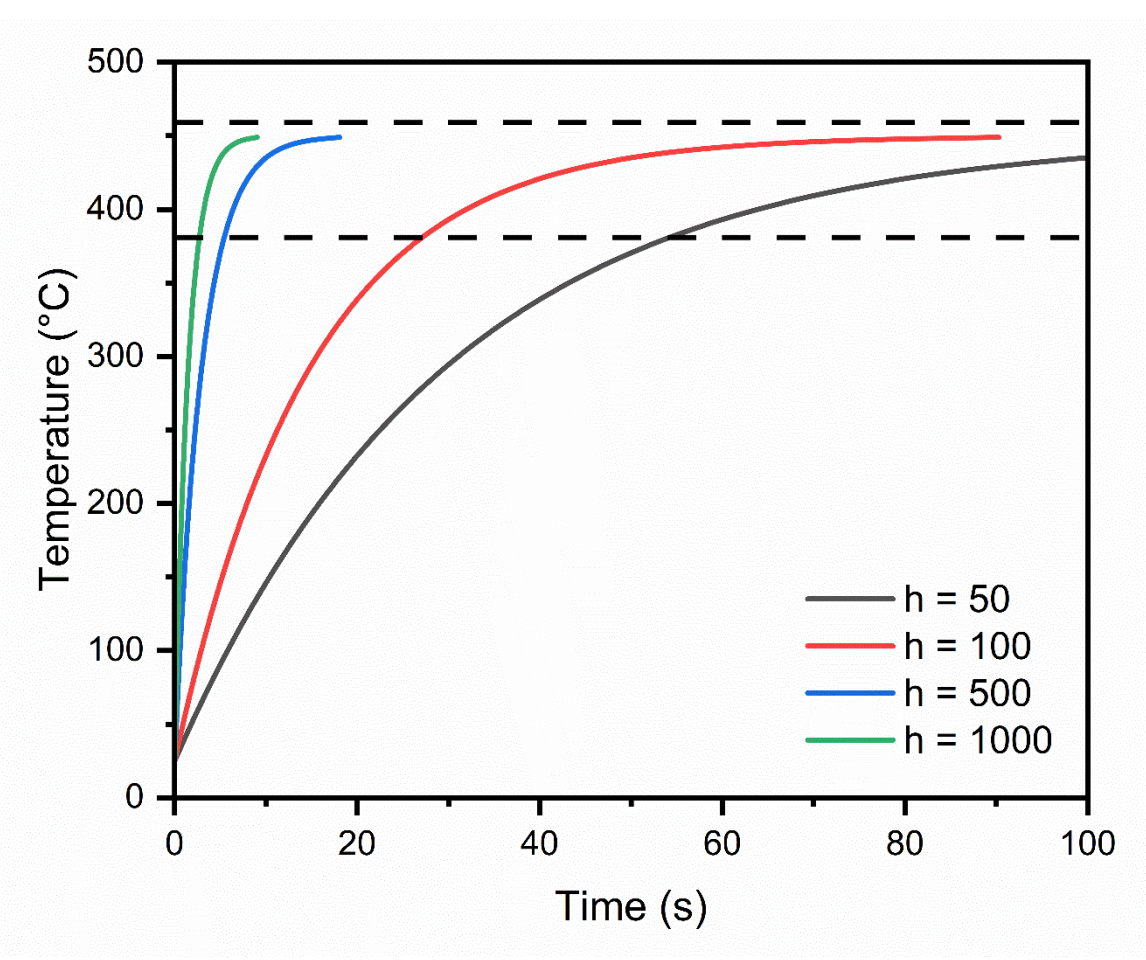


Fig. 3. Plot of temperature as a function of time using lumped capacitance analysis. The horizontal dashed lines demarcate the semi-solid temperature range of the Zn85Al15 alloy. The initial temperature is assumed to be  $25^{\circ}$ C (room temperature). As the value of the heat transfer coefficient h increases, the time required for the wire fragment to reach the semi-solid range decreases.

## **Initial microstructure**

The initial microstructure of the drawn wire prior to heat treatment is shown in Fig. 4. The microstructure consists of alternating phases that are aligned parallel to the drawing direction. The contrast between the phases is achieved using a back-scattered electron detector in an SEM operating at 15kV of accelerating voltage. Fig. 4b provides a magnified view of this microstructure. It is a highly oriented microstructure devoid of dendritic grains and is typical of drawn wires. The small domain size ( $<5\mu m$ ) suggests that the material has undergone phase structure refinement during the multiple drawing processes which is beneficial to produce small globular grains during the heat treatment process. Fig. 4c presents the element distribution map of the initial microstructure. EDS analysis revealed that the lighter phase contained mostly zinc (corresponding to the Zn-rich  $\eta$  phase from the phase diagram, represented by blue) while the darker phases were enriched with aluminum (represented by yellow). The average composition of the darker phase was approximately 24.40 wt% Zn and 75.60 wt% Al, which corresponds to the Al-rich  $\alpha$  phase. The lighter phase had an average composition of 93.43 wt% Zn and 6.57 wt% Al.

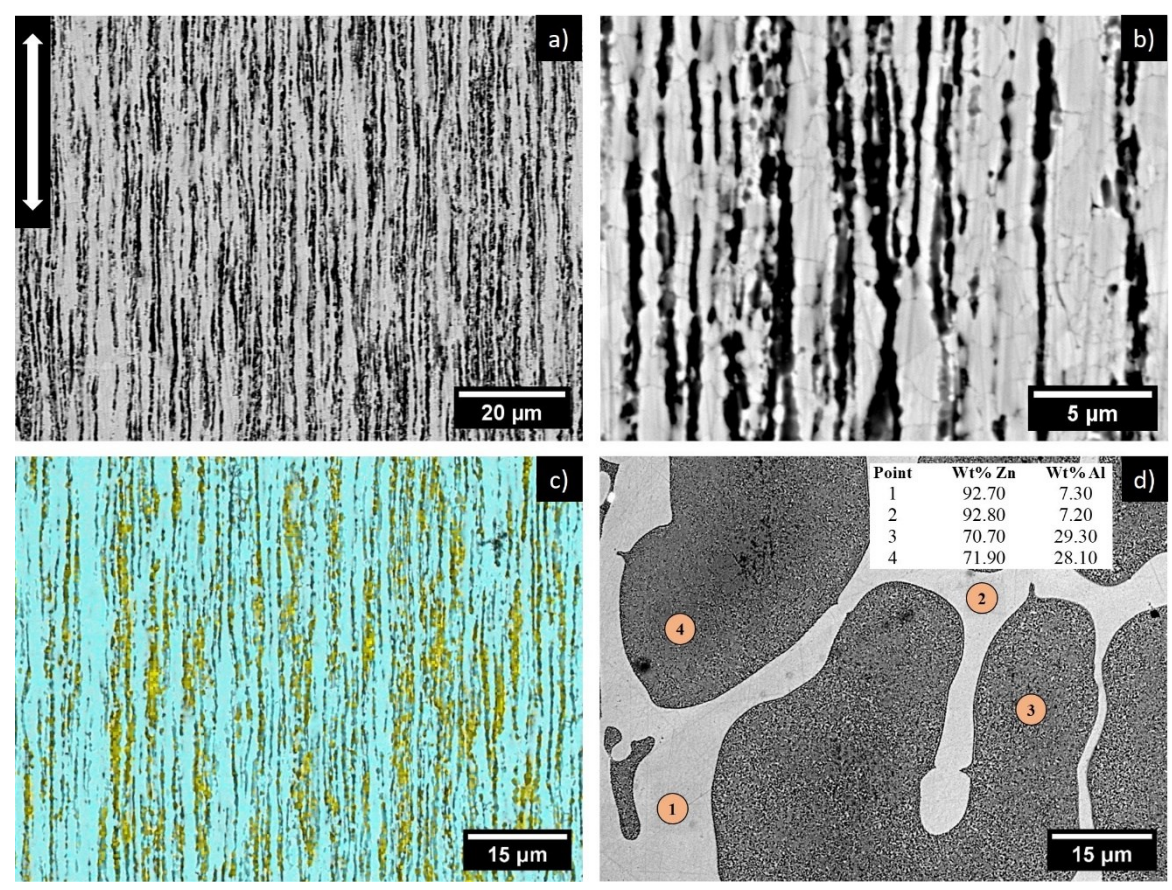


Fig. 4. a, b) Backscattered electron images of the typical microstructure of the drawn wire of the Zn85Al15 alloy. The darker regions correspond to higher concentrations of aluminum compared to the lighter regions; a) The inset arrow indicates the drawing direction; b) Magnified view of the microstructure; c) Element distribution map of the initial microstructure; d) As-cast microstructure of the alloy. The inset table presents the composition at the marked points determined using EDS analysis.

To understand the role of processing in producing this oriented microstructure, we melted some filaments at  $650^{\circ}$ C and cast the melt by pouring into a graphite mold preheated to  $450^{\circ}$ C. The solidifying melt was allowed to air cool for several minutes before quenching it into cold water. Fig. 4d presents the as-cast microstructure together with the EDS analysis. We observed that dendritic grains had formed in the material with an average composition of 71.30 wt% Zn and 28.7 wt% Al. This composition is close to the eutectoid composition of the  $\beta$  phase. The difference between the initial and as-cast microstructure in the compositions and the shape/orientation of phases emphasizes the role of processing in obtaining the desired microstructure. The oriented microstructure likely results from the combination of a continuous casting process to produce the billet and subsequent cold drawing/rolling operations.

#### Globular transformation

The oriented microstructure transformed into a globular microstructure during the heat treatment via a two-step mechanism. The first step comprised of solid-state diffusion resulting in the formation of the  $\beta$  phase from the combination of the  $\alpha$  and  $\eta$  phases through the eutectoid reaction. This transformation was achieved immediately after the temperature of

the wire fragment crossed the eutectoid temperature (277°C). Due to the oriented nature of the initial microstructure, the  $\beta$  phase was formed as bands parallel to the drawing direction. Fig. 5 shows the bands as observed in a quenched sample that was heat treated for 1 minute in a salt bath maintained at 385°C. Although the image provides information in a two-dimensional plane, these bands have a 3-dimensional profile that is rod-like. The EDS analysis of the  $\beta$  phase bands confirmed that their average composition was approximately 73.65 wt% Zn and 26.35 wt% Al. The surrounding liquid (light regions) had an average composition of approximately 93.70 wt% Zn and 6.30 wt% Al.

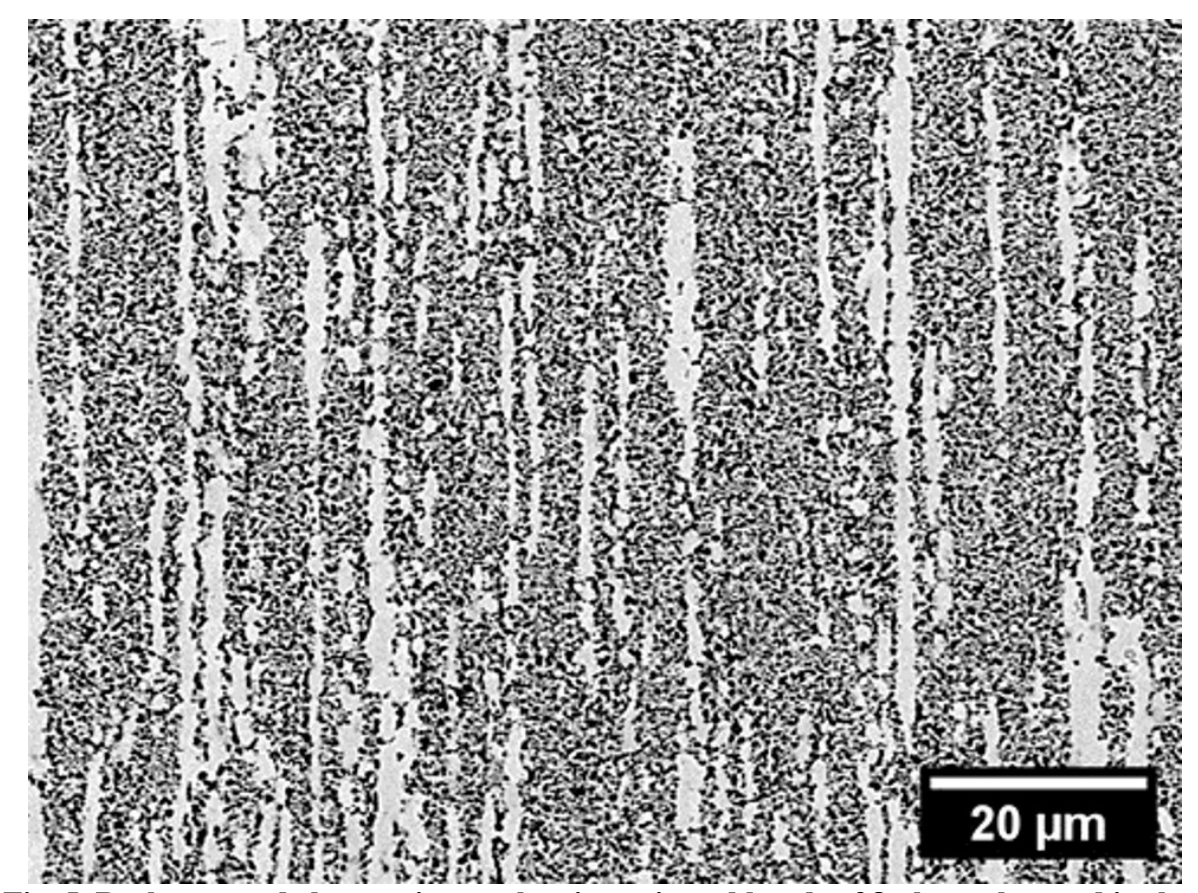


Fig. 5. Backscattered electron image showing oriented bands of  $\beta$  phase observed in the quenched microstructure of a wire fragment heated for 1 minute in a molten salt bath maintained at 385°C.

In the second step, the bands were observed to break up into smaller fragments resulting in globular grains in a liquid matrix. This transformation occurred after the temperature of the wire fragment surpassed the eutectic temperature of the alloy and entered into the semi-solid temperature range. It is supported by visual observation of the wire fragments having the consistency of a cooked pasta strand before quenching. The  $\eta$  phase melted completely to form the liquid phase, together with partial melting of the  $\beta$  phase. The breakup of the  $\beta$  phase bands to form globular fragments can be attributed to the Rayleigh instability phenomenon. In the semi-solid temperature range, the material achieves a viscosity that is largely dependent on the liquid fraction [29]. Under these conditions, perturbations that exist on the surface of the solid bands grow in amplitude and ultimately result in the pinch-off of smaller fragments [30]. These fragments rapidly globularize to minimize the interfacial energy through contact with the surrounding liquid. Fig. 6 illustrates the two-step mechanism for the formation of the globular grains.

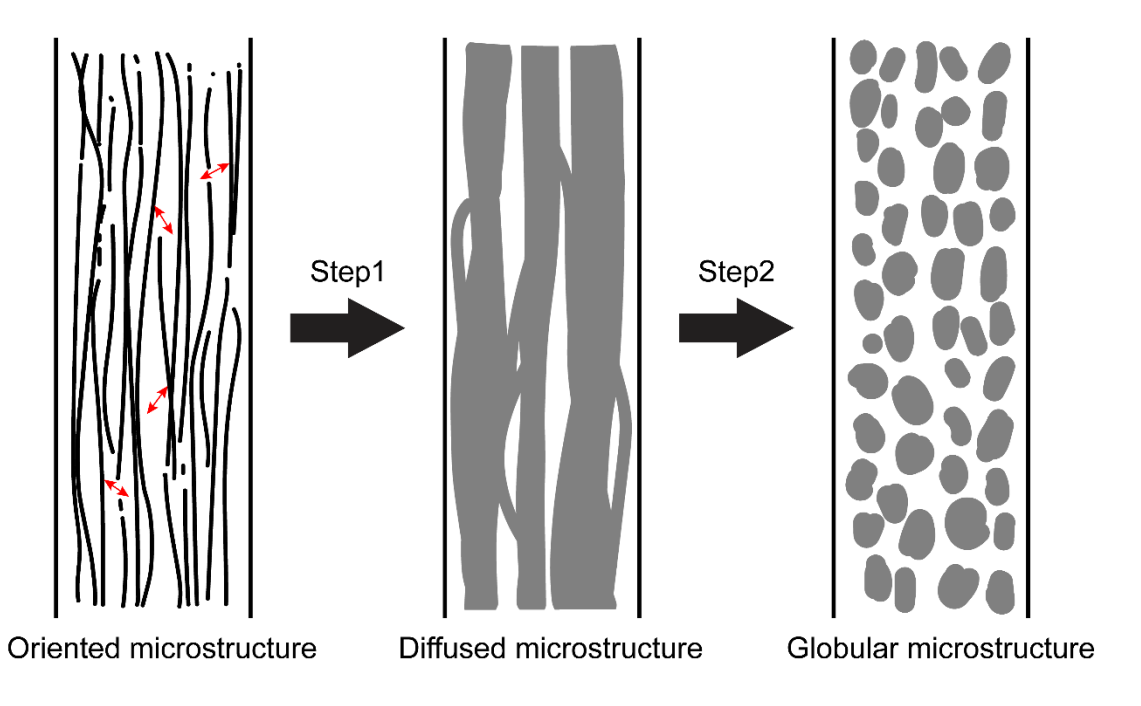


Fig. 6. Illustration of the two-step mechanism for the formation of globular grains. The first step involves solid-state diffusion to form the  $\beta$  phase from the eutectoid combination of the  $\alpha$  and  $\eta$  phases. The red arrows indicate the diffusion of elements between the phases. The second step involves the breakup of the banded structure to form globular fragments through Rayleigh instability.

## Effect of set temperature on globularization time

Rayleigh instability is a kinetic phenomenon. While spheroidization by pinch-off has been demonstrated in solid materials [31,32], the relative timescale of the onset is greatly influenced by the viscosity of the material. The lower the viscosity, the sooner is the onset of the instability and vice versa [33]. A higher viscosity of the surrounding liquid can dampen perturbations on the surface of the band thereby significantly delaying the progression to droplet formation. Since larger liquid fractions result in a lower viscosity, the set temperature of the salt bath and its heat transfer coefficient greatly influence the time required for the globularization process. Under transient heating conditions, a higher set temperature results in rapid increase in the temperature of the wire fragment above the solidus temperature, leading to higher liquid fractions and faster onset of instability. Fig. 7 presents the results from the heat treatment process. At the highest temperature evaluated (450°C), the bands which were formed almost instantaneously started breaking around the 2 second mark (Fig. 7a) and complete separation of grains was observed at 5 seconds (Fig. 7b). At 400 and 420°C, separation of globular grains was achieved around 10 and 20 seconds respectively. When the set temperature was 385°C, the formation of globular fragments took nearly 1.5 minutes. The small difference between the set temperature and solidus temperature (381°C) resulted in slower acquisition of energy above solidus, thereby prolonging melting and delaying the onset of instability. Below the solidus temperature at 375°C, the bands did not break up even after 20 minutes of heat treatment, confirming that viscosity dictates the globularization timescale. The microstructure obtained after quenching this sample is presented in Fig. 8. The EDS results confirm that the bands correspond to the  $\beta$  phase with an average composition of

73.10 wt% Zn and 26.90 wt% Al. The surrounding  $\eta$  phase had an average composition of 93.75 wt% Zn and 6.25 wt% Al.

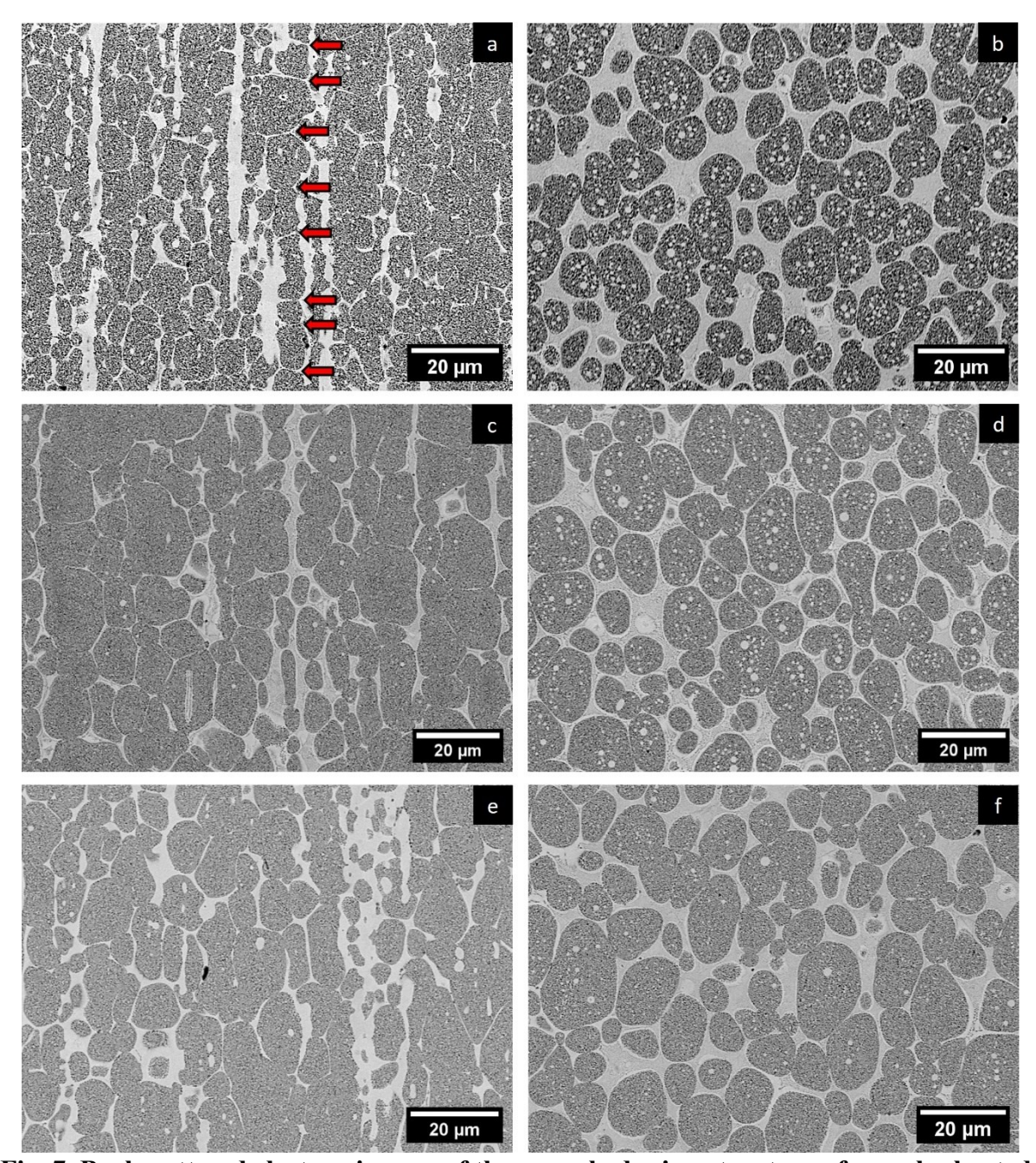


Fig. 7. Backscattered electron images of the quenched microstructure of samples heated in a salt bath maintained at a) 450°C for 2 sec; b) 450°C for 5 sec; c) 420°C for 5 sec; d) 420°C for 10 sec; e) 400°C for 15 sec; and f) 400°C for 20 sec. The arrows indicate the points where the band broke off into smaller segments.

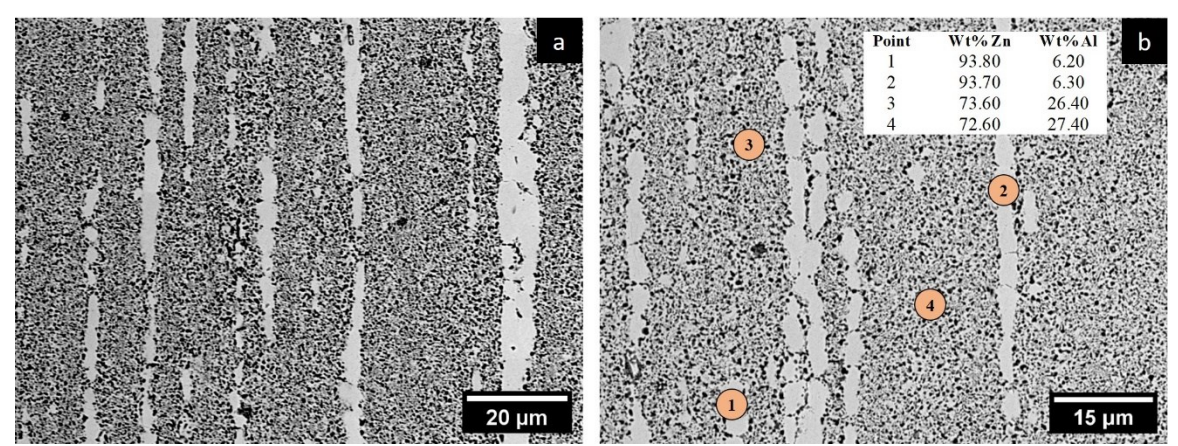


Fig. 8. a, b) Backscattered electron images showing oriented bands of  $\beta$  phase observed in the quenched microstructure of a wire fragment heated for 20 minutes in a molten salt bath maintained at 375°C; b) The inset table presents the composition at the marked points determined using EDS analysis.

# Effect of set temperature on grain size

The set temperature of the salt bath also influenced the size of globular grains formed after breaking up of the bands. Smaller grains were formed when the set temperature was higher. At lower set temperatures, the wire spent a longer time below the solidus temperature in the eutectoid region. This allowed for coarsening of bands through merging to minimize interfacial contact with the adjacent phase. These coarsened bands took longer to break up and resulted in larger fragments. Karim et al. [30] demonstrated that for a given temperature, longer annealing times were required to induce instability in gold nanowires with larger diameters and resulting in larger sphere diameters. At higher bath temperatures, the temperature of the wire quickly crossed the solidus and Rayleigh instability set in rapidly to form small globular grains from thinner bands. The increased partial melting of the β phase with rising temperature also contributed to the formation of smaller grains during breakup. It also explains the higher incidence of liquid pockets inside the grains formed at elevated temperatures (Fig. 7b, 7d). Fig. 9 presents the grain size distribution observed at the different temperatures. Grains smaller than 20µm<sup>2</sup> in area were excluded from the analysis. These fine grains may have originated by nucleation in the liquid phase during quenching and are not representative of the microstructure in the semi-solid state. As the temperature of the salt bath decreased, the median of the distribution gradually shifted towards larger grain sizes.

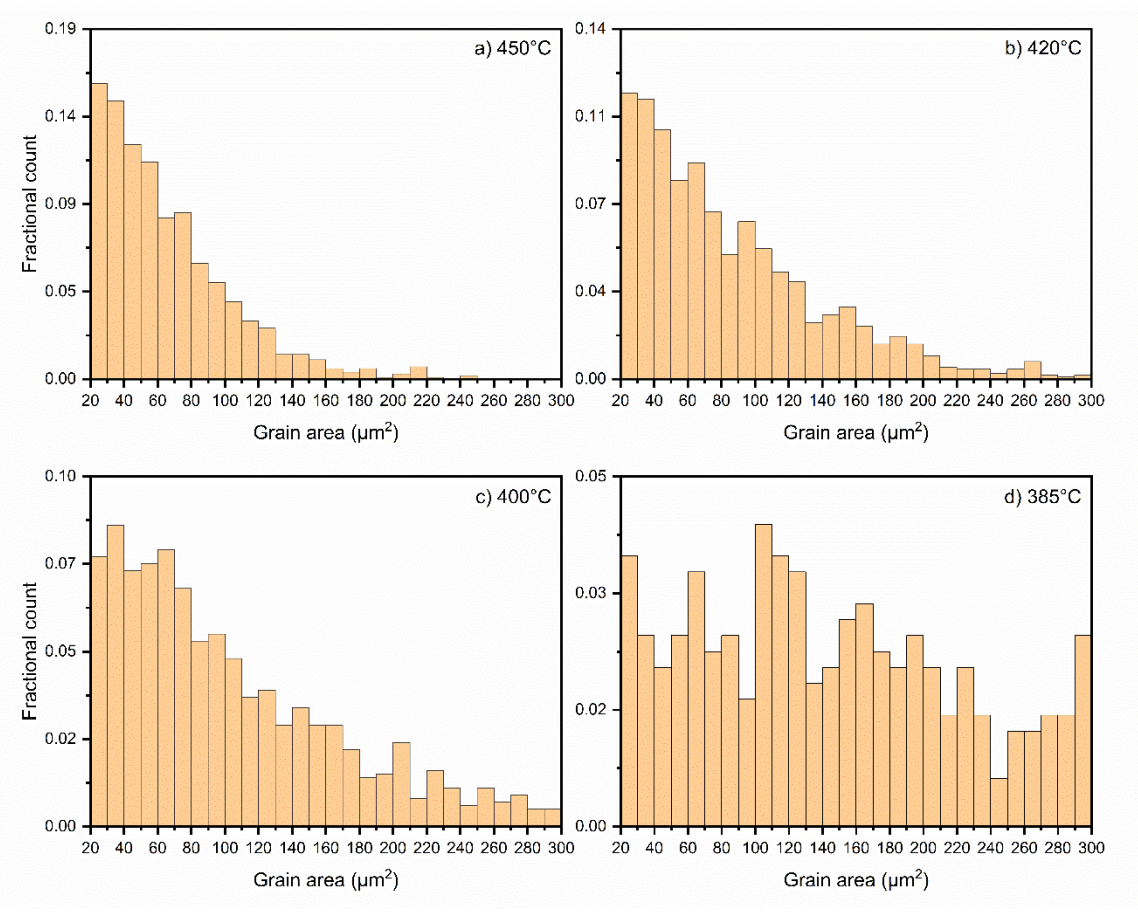


Fig. 9. Plot of the distribution of grain areas upon globular grain formation after heating in a salt bath maintained at a) 450°C for 5 sec; b) 420°C for 10 sec; c) 400°C for 20 sec; and d) 385°C for 1.5 min.

The trends in the time required for globular grain formation and the average size of grains formed is shown in Fig. 10. Both the time required for globularization, and the average size of grains decrease with increasing temperature of heat treatment. Separated globular grains were observed at 5s at 450°C, 10s at 420°C, 20s at 400°C, and 90s at 385°C. The average grain area of the newly formed grains was 65.819μm² at 450°C, 87.141μm² at 420°C, 111.947μm² at 400°C, and 238.873μm² at 385°C. The corresponding grain diameters were 8.798μm at 450°C, 10.004μm at 420°C, 11.230μm at 400°C, and 16.170μm at 385°C. The timescale for the onset of Rayleigh instability in a cylinder may be understood in terms of the equation [34]–

$$\frac{\partial n}{\partial t} = \frac{D_s \gamma \Omega^2 v}{kT y} \frac{\partial}{\partial s} \left( y \frac{\partial K}{\partial s} \right) \tag{5}$$

where  $\frac{\partial n}{\partial t}$  is the normal velocity of the surface at the point of interest,  $D_s$  is the surface self-diffusion coefficient,  $\gamma$  is the surface tension,  $\Omega$  is the atomic volume, v is the number of diffusing atoms per unit surface area, k is the Boltzmann's constant, T is the temperature, y is the radius of the cylinder, s is the arc length along the generating curve for the surface, and K is the surface curvature gradient.

We find that the characteristic time for Rayleigh instability to occur largely depends on temperature since it also influences the surface tension and diffusion coefficients. By

converting the above equation into its dimensionless form and solving, one may also obtain that pinch-off time drastically reduces as the radius of the cylinder is decreased, other values remaining constant.

Once the globular grains were formed, grain coarsening was observed to occur due to Ostwald ripening. The average grain area and diameter calculated after 15 seconds at 420°C were 96.258µm² and 10.488µm respectively. Similarly at 400°C, the values were determined to be 153.736µm² and 13.061µm after 30 seconds of heating. The mean circularity of the grains also improved slightly with increasing temperature. The average circularity of the newly formed globular grains was determined to be 0.756 at 385°C, 0.781 at 400°C, 0.795 at 420°C and 0.799 at 450°C. These values clearly indicate that the microstructure obtained after heat treatment is thixotropic and suitable for additive manufacturing processes.

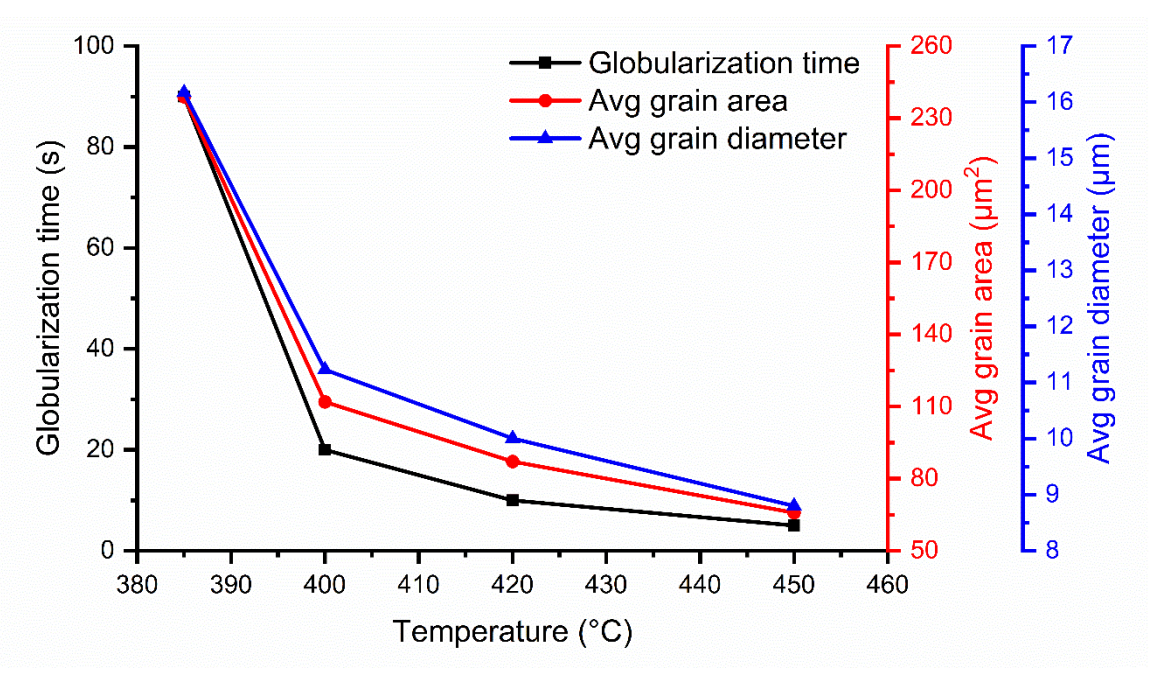


Fig. 10. Plot of the time required for globular grain formation, average grain area, and average grain diameter as a function of temperature. As the set temperature of the heating bath increases, smaller grains are formed more rapidly from the breakup of the bands.

# **Conclusions**

In this study, a rapid thermal treatment was performed on cold-drawn wires of a Zn-Al alloy. The objective was to generate fine globular grains in the semi-solid condition to make the material thixotropic. The alloy composition was selected based on thermodynamic criteria for thixoforming processes. Analysis of microstructures in the quenched condition revealed that for alloy compositions undergoing a eutectoid transformation, an oriented microstructure in the starting material would promote the formation of globular grains during partial melting due to Rayleigh instability. Higher heat transfer coefficients of molten salt baths reduce the time required to heat materials to the semi-solid temperature range. A higher set temperature also influences the early onset of instability in the bands and results in smaller grains. Prolonged heating after globular grain formation coarsens the grains due to Ostwald ripening and may be minimized by carefully controlling the heating time. Overall, small globular grains (~10µm) having a high mean circularity (>0.75) were successfully produced in the

heat-treated wires. Therefore, a rapid pretreatment at elevated temperatures could serve as an effective method to prepare a thixotropic filament from drawn wires for fine resolution 3D printing.

## Acknowledgements

This material is based upon work supported by the National Science Foundation under Grant Nos. 2027871 and 2027823. Any opinions, findings, and conclusions or recommendations expressed in this material are those of the authors and do not necessarily reflect the views of the National Science Foundation.

# **Conflict of interest**

The authors declare no conflict of interest.

## References

- [1] S. Deepak Kumar, J. Ghose, and A. Mandal, *Sustainable Engineering Products and Manufacturing Technologies*, ed. K. Kumar, D. Zindani, and J.P. Davim (Elsevier, Amsterdam, 2019), p. 25.
- [2] S. Ji, K. Wang, and X. Dong, Crystals (2022). https://doi.org/10.3390/cryst12081044
- [3] S.D.E. Ramati, G.J. Abbaschian, and R. Mehrabian, *Metall. Mater. Trans. B* (1978). https://doi.org/10.1007/BF02653689
- [4] D.H. Kirkwood and P. Kapranos, Semisolid Processing. *Mater. Sci. Mater. Eng.* (2016). https://doi.org/10.1016/B978-0-12-803581-8.03585-2
- [5] C.G. Kang, C.K. Jin, and A. Bolouri, *Procedia Eng.* (2014). https://doi.org/10.1016/j.proeng.2014.09.129
- [6] C.S. Rice, P.F. Mendez, and S.B. Brown, *JOM* (2000). <a href="https://doi.org/10.1007/s11837-000-0065-5">https://doi.org/10.1007/s11837-000-0065-5</a>
- [7] Z. Chang, N. Su, Y. Wu, Q. Lan, L. Peng, and W. Ding, *Mater. Des.* (2020). https://doi.org/10.1016/j.matdes.2020.108990
- [8] B. Binesh, M. Aghaie-Khafri, M. Shaban, and A. Fardi-Ilkhchy, *Int. J. Mater. Res.* (2018). https://doi.org/10.3139/146.111710
- [9] Q.Q. Zhang, Z.Y. Cao, Y.F. Zhang, G.H. Su, and Y.B. Liu, *J. Mater. Process. Technol.* (2007). <a href="https://doi.org/10.1016/j.jmatprotec.2006.11.022">https://doi.org/10.1016/j.jmatprotec.2006.11.022</a>
- [10] B. Binesh and M. Aghaie-Khafri, *Mater. Des.* (2016). https://doi.org/10.1016/j.matdes.2016.01.117
- [11] Y. Xu, L. Hu, J. Jia, and B. Xu, *Mater. Charact.* (2016). https://doi.org/10.1016/j.matchar.2016.06.011
- [12] Q. Tang, M. Zhou, L. Fan, Y. Zhang, G. Quan, and B. Liu, *Vacuum* (2018). https://doi.org/10.1016/j.vacuum.2018.06.053

- [13] G. Xiao, J. Jiang, Y. Liu, Y. Wang, and B. Guo, *Mater. Charact.* (2019). https://doi.org/10.1016/j.matchar.2019.109874
- [14] C. Chaussê de Freitas, K.N. Campo, and R. Caram, *Vacuum* (2020). <a href="https://doi.org/10.1016/j.vacuum.2020.109567">https://doi.org/10.1016/j.vacuum.2020.109567</a>
- [15] K.N. Campo, C.T.W. Proni, and E.J. Zoqui, *Mater. Charact.* (2013). https://doi.org/10.1016/j.matchar.2013.08.011
- [16] M.S. Salleh, M.Z. Omar, J. Syarif, K.S. Alhawari, and M.N. Mohammed, *Mater. Des.* (2014). <a href="https://doi.org/10.1016/j.matdes.2014.07.014">https://doi.org/10.1016/j.matdes.2014.07.014</a>
- [17] H. Guo and X. Yang, *Trans. Nonferrous Met. Soc. China* (2007). https://doi.org/10.1016/S1003-6326(07)60177-0
- [18] A. Alharbi, A. Khan, I. Todd, M. Ramadan, and K. Mumtaz, *Mater. Today: Proc.* (2021). https://doi.org/10.1016/j.matpr.2021.05.549
- [19] A. Jabbari and K. Abrinia, JOM (2019). https://doi.org/10.1007/s11837-018-3282-5
- [20] A. Jabbari and K. Abrinia, *J. Manuf. Process.* (2018). https://doi.org/10.1016/j.jmapro.2018.08.031
- [21] D.D. Lima, K.N. Campo, S.T. Button, and R. Caram, *Mater. Des.* (2020). https://doi.org/10.1016/j.matdes.2020.109161
- [22] N. Nezic, M. Speth, K. Rouven Riedmüller, and M. Liewald, *Mater. Res. Proc.* (2023). https://doi.org/10.21741/9781644902479-9
- [23] "Zinc Alloys Material Properties Zinc-Aluminum 12." <a href="https://www.makeitfrom.com/material-properties/Zinc-Aluminum-12-ZA-12-Z35631">https://www.makeitfrom.com/material-properties/Zinc-Aluminum-12-ZA-12-Z35631</a> (accessed Dec. 17, 2023).
- [24] A. Pola, M. Tocci, and F.E. Goodwin, *Metals* (2020). https://doi.org/10.3390/met10020253
- [25] J. Wojtkowiak, *Lumped Thermal Capacity Model*, ed. R.B. Hetnarski (Springer, Dordrecht, 2014), p. 2808.
- [26] D. Liu, H.V. Atkinson, and H. Jones, *Acta Mater.* (2005). https://doi.org/10.1016/j.actamat.2005.04.028
- [27] A.M. Camacho, H.V. Atkinson, P. Kapranos, and B.B. Argent, *Acta Mater.* (2003). https://doi.org/10.1016/S1359-6454(03)00040-5
- [28] Y.Q. Liu, A. Das, and Z. Fan, *Mater. Sci. Technol.* (2004). https://doi.org/10.1179/026708304225011973
- [29] O. Lashkari and R. Ghomashchi, *J. Mater. Process. Technol.* (2007). https://doi.org/10.1016/j.jmatprotec.2006.08.003
- [30] S. Karim, M.E. Toimil-Molares, A.G. Balogh, W. Ensinger, T.W. Cornelius, E.U. Khan, and R. Neumann, *Nanotechnology* (2006). https://doi.org/10.1088/0957-4484/17/24/009
- [31] W.A. Jensen, N. Liu, E. Rosker, B.F. Donovan, B. Foley, P.E. Hopkins, and J.A. Floro, *J. Alloys Compd.* (2017). https://doi.org/10.1016/j.jallcom.2017.06.023

[32] B. Chanda, S.K. Pani, and J. Das J, *Mater. Sci. Eng. A* (2022). https://doi.org/10.1016/j.msea.2022.142669

[33] M. Rombouts, J.P. Kruth, L. Froyen, and P. Mercelis, *CIRP Ann.* (2006). https://doi.org/10.1016/S0007-8506(07)60395-3

[34] F.A. Nichols and W.W. Mullins, J. Appl. Phys. (1965). https://doi.org/10.1063/1.1714360